Auralization of a Supersonic Business Jet Using Advanced Takeoff Procedures

Stephen A. Rizzi[1]
NASA Langley Research Center, Hampton, VA 23681, USA

Jeffrey J. Berton[2]
NASA Glenn Research Center, Cleveland, OH 44135, USA

Brian C. Tuttle[3]
Analytical Mechanics Associates, Inc., Hampton, VA 23681, USA

Recent NASA studies of a supersonic business jet airplane indicated that advanced takeoff procedures could be used to reduce noise at the lateral sideline location to a level at which Chapter 4 noise certification requirements could be met. The studies were conducted with the NASA Aircraft Noise Prediction Program, using an analytical model of the airframe and its engines. The advanced procedure consists of a higher-speed climbout and a programmed thrust lapse in which the engine thrust is automatically and gradually reduced immediately after the runway obstacle is cleared. In this paper, the authors utilize the results of the most recent study as the basis of an auralization of the predicted noise. Modifications to the NASA Auralization Framework necessary for that process are described. The auralizations are used to demonstrate differences between standard and advanced takeoff procedures, beyond those that may be observed through comparison of integrated noise metrics.

I. Introduction

IN addition to sonic boom,[1] several barriers exist to certification of commercial supersonic aircraft. Chief among them is the problem of community noise in the vicinity of airports, resulting primarily from high jet noise on takeoff. Standards and reference procedures pertaining to civil supersonic airplane noise are expected to be based, in part, upon those for subsonic transports. The introduction of high bypass ratio turbofan engines over the last few decades has significantly reduced jet noise of subsonic aircraft. However, that engine cycle design and architecture are not viable for supersonic aircraft because such aircraft require higher specific thrust engines with lower cross-sectional area for supersonic cruise. Therefore, alternative measures must be sought to reduce the community noise to a level that supersonic aircraft can certify under subsonic requirements.

A recent NASA study of a supersonic business jet airplane indicated that the introduction of advanced takeoff procedures could reduce the noise at the most challenging of the three noise certification points, that is, the lateral or sideline point, to a level at which the Chapter 4 noise regulations could be met.[2] These regulations apply to smaller aircraft under 55 tonnes and remain in effect for new aircraft applicants until December 2020. A sketch of the three noise certification points (lateral, flyover, and approach) is shown in Figure 1. The takeoff procedure involves an automatic reduction in the engine thrust following clearance of the runway obstacle requirement. The so-called programmed thrust lapse takeoff[3] reduces the thrust gradually from the maximum thrust, in contrast to the more abrupt pilot-initiated cutback prior to the flyover certification point. In combination with a higher-speed climbout, the predicted noise was reduced to the point at which the Chapter 4 requirements could be met, both on a cumulative and per certification point basis. The NASA Aircraft Noise Prediction Program (ANOPP)[4] was used for the system noise prediction.

[1] Senior Researcher for Aeroacoustics, Aeroacoustics Branch, AIAA Fellow
[2] Aerospace Engineer, Propulsion Systems Analysis Branch, AIAA Senior Member
[3] Scientist III

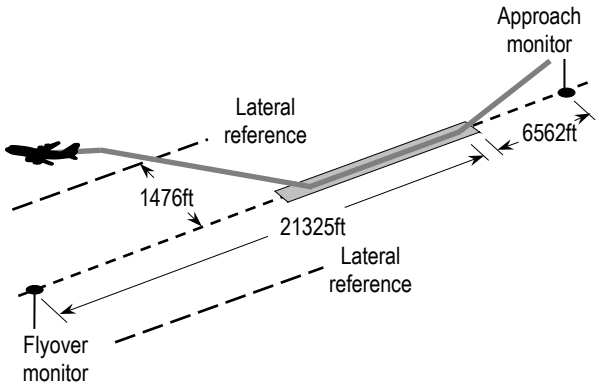

Figure 1: Noise certification points relative to takeoff and landing flight paths.

While the reduction in noise from the standard takeoff procedure can be described in terms of the effective perceived noise level (EPNL) metric used for certification, that time-integrated metric may not effectively communicate the noise impact to nonacousticians. The auralization of aircraft flyover noise, that is, the process by which numerical predictions are converted into sounds that can be heard, has been shown to be an effective tool for doing so.[5] In this work, the NASA Auralization Framework (NAF)[6] is used for this purpose. The NAF uses the source data generated by the system noise prediction as its starting point, synthesizes the sound, and propagates that sound to a ground observer.

In this paper, the system noise predictions performed in a companion study[7] are briefly summarized. This more recent study is a continuation of the prior work[2] and more broadly assesses performance, noise, and exhaust emissions. The auralization process is next described, including the development of a new software plugin for atmospheric absorption according to the SAE ARP 866A standard,[8] conversion of the system noise predictions from ANOPP to NASA's second generation Aircraft Noise Prediction Program (ANOPP2) framework,[9] and a number of other practical considerations. Finally, auralizations of standard and advanced takeoff procedures are performed to highlight acoustic differences between the two procedures. There was no attempt to auralize the single approach condition considered in the companion study. Comparisons of integrated noise metrics from the takeoff auralizations with those obtained from the system noise prediction are used to verify results. Sound quality metrics are computed, and an annoyance model is exercised to provide additional insight into possible human response.

II. System Noise Prediction

A. Concept Vehicle Description

A supersonic technology concept airplane (STCA) with a maximum gross weight of just under 55 tonnes was selected for this study. Engines were designed for a Mach 1.4 cruise at 50 kft. Three engines are needed to provide sufficient thrust for cruise for a lift-to-drag ratio of roughly 8. The engines were assumed to be mounted on short aft fuselage pylons above the wing to shield forward-radiating fan noise from ground observers during takeoff and landing. The nozzle exit planes extended aft of all airframe surfaces; thus, aft-radiating fan noise, core noise, and jet noise do not benefit from wing shielding. A model of the vehicle concept is shown in Figure 2, with aircraft characteristics provided in Table 1.

The engines were derived from an existing subsonic turbofan engine instead of a clean sheet design, in order to be ready for testing by 2025. The low-pressure spool of a CFM56-7B was redesigned for Mach 1.4 cruise; the booster was discarded; and the fan and low-pressure turbine were redesigned for a higher pressure ratio. The Numerical Propulsion System Simulation (NPSS) code[10] was used to predict engine performance. The reader is referred to the companion paper[7] for additional details on the STCA engine and airframe.

B. Takeoff Procedures

Two takeoff procedures were considered: standard and advanced. Both procedures utilize a delayed rotation, allowing the aircraft to operate well above its minimum takeoff safety speed (V_{2min}) of 177 knots (kt) and closer to its minimum drag speed. A delayed rotation allows for higher rotation, liftoff, and climbout speeds with lower thrust. The procedures are summarized below, with additional details provided in the companion paper.[7]

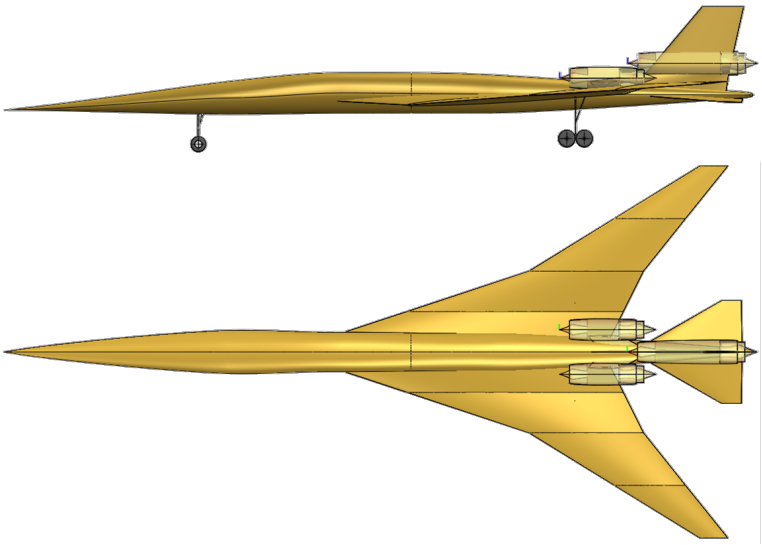

Figure 2: Solid model of the 55 tonne trijet concept.[7]

Table 1: 55t trijet characteristics.[7]

Max takeoff weight (klb)	121
Passengers	8
Cruise Mach	1.4
Engines (x3)	CFM56-derived
Overall length (ft)	135
Span (ft)	67
Wing reference area (ft^2)	1619
Wing aspect ratio	2.7
Wing taper ratio	0.09
Wing loading (lb/ft^2)	74
Wing fuel (klb)	24
Fuselage fuel (klb)	36
Fuel fraction	0.50

1. Standard Takeoff Procedure

A takeoff calculation for noise certification from a sea level field on a standard acoustic day, International Standard Atmosphere (ISA)+18°F, was made in accordance with the requirements for subsonic transports in chapter 3.6.2 of Annex 16.[11] Above the minimum safe altitude, engine power is reduced during a pilot-initiated cutback such that the climb gradient is zero with one engine inoperative, or four percent with all engines operating. The engine power cutback is designed to reduce noise at the flyover monitor. In this study, the cutback is complete 18 kft from brake release, so that the noise at the flyover monitor is determined entirely by the cutback power noise signature. The standard takeoff procedure is depicted for a steady climbout in the left side of Figure 3. It is permissible without departure from normal procedures for subsonic airplanes, which require applicants to climb at airspeeds no greater than 20 kt above the takeoff safety speed, that is, the "not greater than V_2 plus 20 kt" requirement defined by chapter 3.6.2(d)(1) of Annex 16.[11]

2. Advanced Takeoff Procedure

A noise certification takeoff using a programmed thrust lapse rate of 10% is shown on the right side of Figure 3. Immediately after the runway obstacle is cleared (but well before the conventional, pilot-initiated cutback takes place), engine thrust is automatically lowered to reduce lateral (sideline) noise. The reduction is completed by the start of the second segment climb. In this procedure, the airplane climbs out at V_2 + 35 kt. Such a high-speed climbout would require a departure from chapter 3.6.2(d)(1) of Annex 16,[11] with the justification that it may be required to ensure adequate thrust margin and climb performance.

Advanced takeoff procedures have several positive impacts on noise, in addition to reducing lateral noise. A high-speed climbout results in less shear between the jet and ambient air, resulting in less jet noise. It also results in generally lower integrated noise due to shorter event duration and allows for a deeper pilot-initiated engine thrust cutback because of increased lift (compare the lower left and right plots in Figure 3). However, both a programmed thrust lapse and a high-speed climbout result in lower altitudes over the flyover monitor.

C. Noise Modeling

Noise predictions in the companion paper[7] were made using the NASA ANOPP, with engine state data computed by NPSS as functions of flight speed, altitude, and engine power setting. Engine and airframe source noise components and noise suppressions were computed according to the semiempirical methods indicated in Table 2. Engine noise sources included jet, core, and inlet and exhaust fan broadband and rotor-stator interaction tones. Airframe noise sources included main and nose landing gear, leading edge slat, trailing edge flap, and wing and horizontal tail trailing edge noise. Suppressions to isolated source noise data are also listed in Table 2. At maximum power only, an additional adjustment of -2.3 dB was applied to all components to account for estimated engine-by-engine shielding and refraction-scattering at a typical 30° lateral elevation angle.

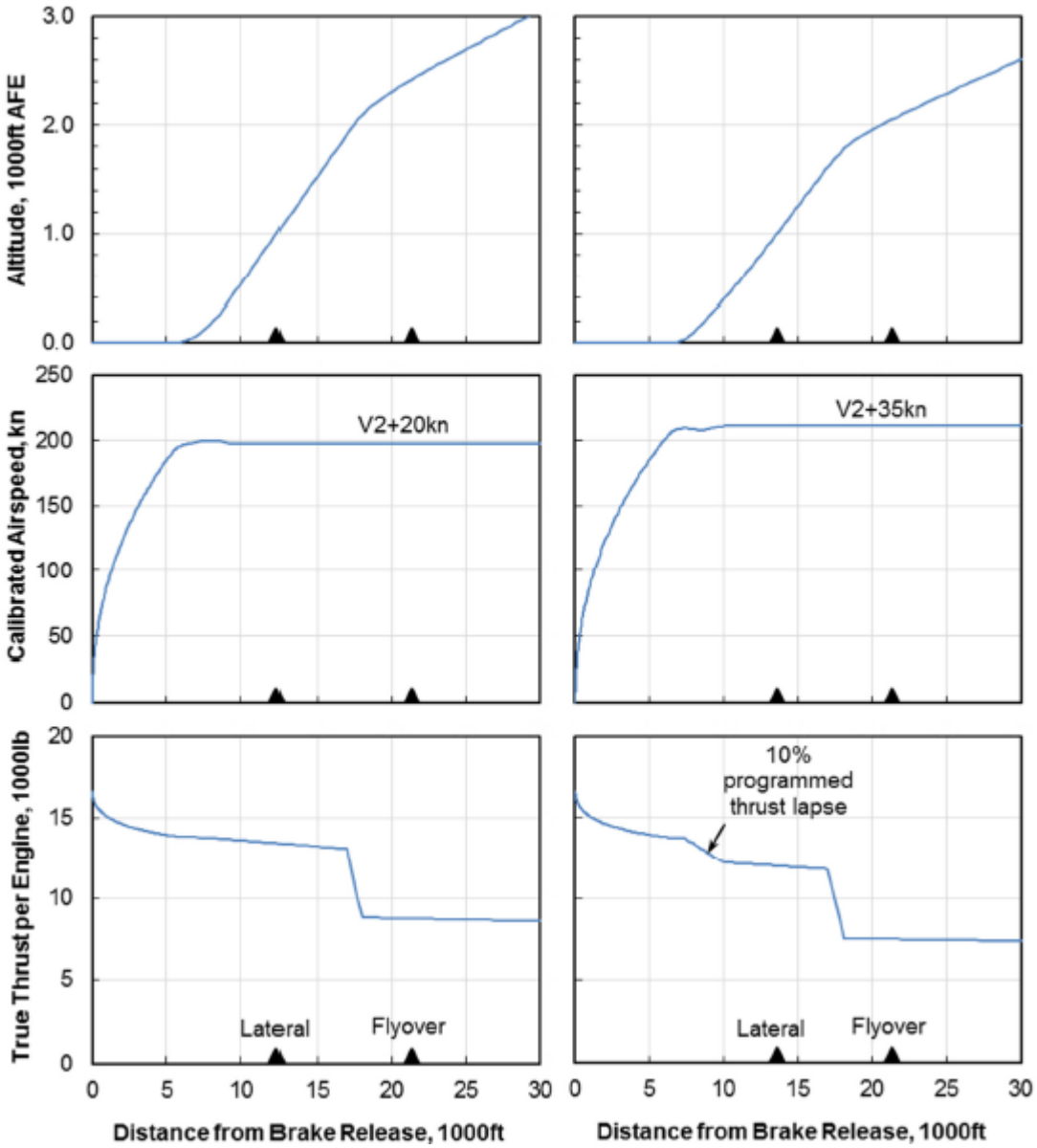

Figure 3: STCA profiles of standard takeoff (left) and advanced takeoff (right) conditions.[7]

Table 2: ANOPP prediction modules and synthesis methods used for auralization.

Component	ANOPP[4] Module	Suppressions	Synthesis Method[5]
Jet	SAE[12]	–	Broadband
Fan Broadband	HDNFAN[13]	Fan Liner (forward & aft)[14] ANOPP WING (forward)[15]	Broadband
Fan Rotor-Stator Interaction Tones	HDNFAN[16]	Fan Liner (forward & aft)[14] ANOPP WING (forward)[15]	Tonal
Core	GECOR[17]	–	Broadband
Airframe	FNKAFM[18]	Delta-wing[19,20]	Broadband

Noise levels of all components were predicted as lossless, one-third octave band spectra. The noise sources were analytically flown along the trajectories described in Section II.B, and were propagated to noise monitors located at 4 ft above the ground. The source levels were computed at one-half-second intervals using engine state data at the

correct flight condition and engine power. This is particularly important in modeling noise during procedures where the engine state is dynamically varying, such as during the programmed thrust lapse procedure. Noise propagation effects included spherical spreading, Doppler shift and convective amplification, atmospheric absorption,[8] and ground reflections[21] based on data for grass-covered ground.[22] Lateral (sideline) noise levels were evaluated lateral to the downrange point at which the aircraft reached 1000 ft above ground level.

D. Noise Predictions

Predicted tone corrected perceived noise data (PNLT) at the 4 ft observer are shown in Figure 4 and Figure 5 for the standard takeoff at the lateral and flyover certification points, respectively. The plots also show the polar emission angle at the time of reception (90 deg directly below the source). The location of each point is depicted in Figure 1, with the lateral point 12,325 ft downrange of brake release. At both points, the jet noise component is dominant; the next highest noise component (core noise) is about 16 dB down from the total at the lateral point, and about 13 dB down at the flyover point. Shielding of the fan inlet noise by the wing is highly effective. When unshielded (not shown), the peak level is comparable to that of the combined airframe noise at both the lateral and flyover points. That is greater than 20 dB and 30 dB above the shielded configuration at the lateral and flyover points, respectively. The dip seen at about 70 s at the flyover point corresponds to the pilot-initiated cutback.

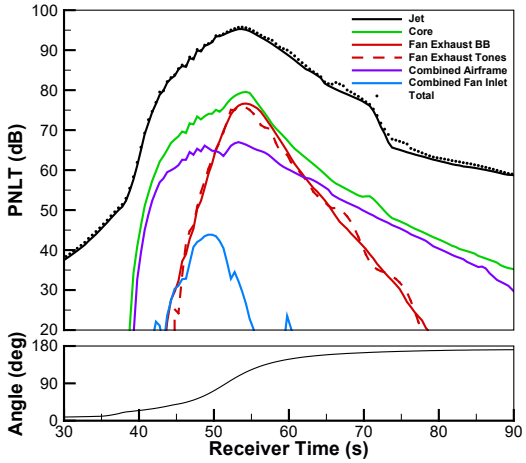

Figure 4: Predicted PNLT for a standard takeoff at the lateral certification point.

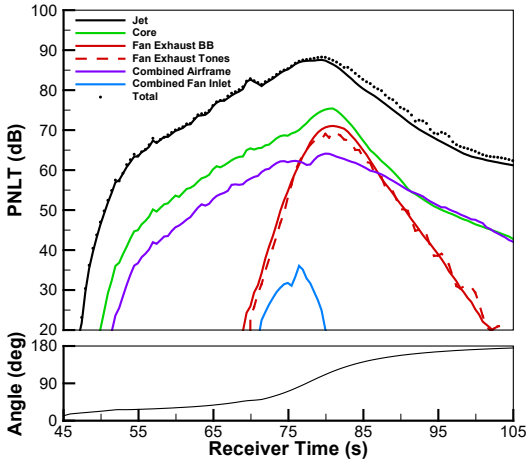

Figure 5: Predicted PNLT for a standard takeoff at the flyover certification point.

In contrast, predicted PNLT data for the advanced takeoff with a programmed thrust lapse of 10% and a higher-speed climbout are shown in Figure 6 and Figure 7 at the lateral and flyover certification points, respectively. The lateral point for the advanced takeoff procedure is located 13,550 ft from brake release. The maximum PNLT is reduced by 1.8 dB at the lateral point and by 0.5 dB at the flyover point relative to the standard takeoff, indicating the effectiveness of the advanced takeoff in reducing lateral noise. The source noise breakdown is comparable to that of the standard takeoff, and is dominated by jet noise. Note also that the emission angle profiles differ from those of the standard takeoff due to the differing speeds and rates of climb. The small dip at the flyover point between about 46 – 48 s corresponds to the rotation point. This dip is not visible in Figure 5 because it occurs before 45 s receiver time. This feature appears as the knee in the jet noise and total noise traces at about 41 s at the lateral point, a feature that is apparent in both the standard (Figure 4) and advanced (Figure 6) takeoff procedures. A dip in level corresponding to the 10% programmed thrust lapse is not apparent at the flyover point, between about 49 – 54 s, or at the sideline point, between about 42 – 47 s.

Integrated metrics in the form of the effective perceived noise level (EPNL), the applicable noise certification metric, are provided in Table 3. It is seen that the difference between the standard and advanced takeoff for the lateral certification point is just slightly more (0.2 dB) than the difference in the peak PNLT, indicating that the shorter duration of the high-speed climbout of the advanced takeoff has marginal benefit on lateral EPNL. In contrast, a greater difference is found at the flyover point (1.6 dB in EPNL vs 0.5 dB in PNLT), indicating that the shorter duration of the high-speed climbout has a greater effect at the flyover point. Table 3 also shows high levels on approach, due to the high thrust needed at low speed, the cumulative levels over the three certification points, and the cumulative margin relative to the applicable Chapter 4 limit for subsonic aircraft. The latter measure highlights the benefits of the advanced takeoff procedure.

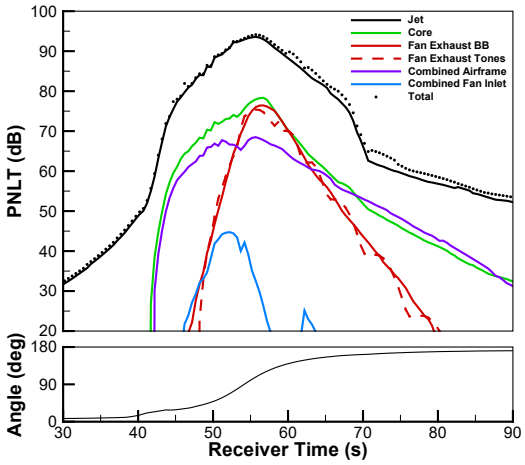

Figure 6: Predicted PNLT for an advanced takeoff at the lateral certification point.

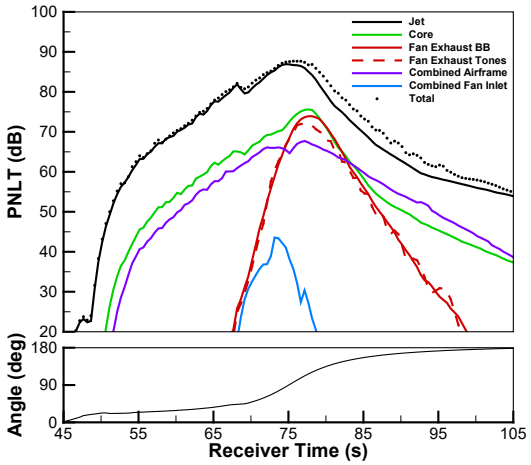

Figure 7: Predicted PNLT for an advanced takeoff at the flyover certification point.

Table 3: EPNL predictions (dB).[7]

Certification Point	Standard Takeoff	Advanced Takeoff
Lateral	95.0	93.0
Flyover	88.6	87.0
Approach	96.4	96.4
Cumulative / Margin (rel. Chapter 4)	280.0 / -2.0	276.4 / 1.6

III. Auralization Framework

The NAF[6] is a collection of dynamic link libraries with functions and data structures common to auralization. Users of the NAF write their own application code, using the NAF Application Programming Interface (API). The typical use case is a time marching simulation, with the main operations depicted in Figure 8. At each time step, the NAF Path Finder first determines the path(s) between the source and receiver at emission time. Here, a source refers to one or more colocated components (e.g., an engine source consisting of jet, core, and fan components). The emission angle(s) are calculated and passed to the NAF synthesis engine, where the component noise definition data (e.g., noise hemispheres) are interpolated and synthesized to produce a segment of pressure time history data at the source for the current time increment. In parallel with the synthesis operation, the NAF Path Traverser determines the attenuation associated with spherical spreading, the delay associated with the propagation time, and spectral modification associated with the atmospheric absorption and ground reflection, along each path. These are represented as a series of gains, time delays, and filters (GTF) that propagate the synthesized signals in the time domain to generate the pressure time history at the observer, referred to as the pseudorecording.

The NAF itself provides basic auralization capabilities. Its open architecture allows users to write their own libraries for additional functionality. The NASA-developed NAF Advanced Plugin Library (NAF-APL) provides additional capabilities for noise synthesis, path finding, and path traversal. Several of these are utilized in the current work, including broadband and tonal noise synthesis, ground plane impedance, and atmospheric absorption.

A. New NAF Developments

Prior to this work, there were two choices for implementing atmospheric absorption in the NAF; a basic user-specified constant absorption in dB/unit length at each one-third octave band center frequency (applicable only to a uniform atmosphere), and an atmospheric absorption model incorporated in the NAF-APL, following the ANSI S1.26-1995 standard.[23] For consistency with the companion paper,[7] a new plugin for the SAE ARP 866A atmospheric absorption model[8] was developed and added to the NAF-APL. The SAE model evaluates the absorption at the one-third octave band center frequencies below 4 kHz, and at the lower limit of each one-third octave band above 4 kHz. A comparison of the propagated noise using the ANSI and SAE methods is made in Section IV. Irrespective of the

particular absorption model, the accumulated absorption along the path is converted to a finite impulse response (FIR) filter,[24] and applied to the sample buffer by the GTF processor.

B. Coupling ANOPP2-NAF Frameworks

As indicated in Section II.C, the ANOPP analyses were performed such that the source levels were computed at one-half-second intervals using engine state data at the correct flight condition and engine power. Effectively, this translates into hundreds of waypoints during the course of a takeoff procedure, and necessitates an automated means of transferring the source noise definitions and other information to the NAF. The ANOPP2-NAF Interface Library[25] was built expressly for this purpose.

Like the NAF, the ANOPP2 framework[9] consists of a set of libraries and associated APIs. Users write their own ANOPP2 application code based on the particular analysis requirement. In contrast, ANOPP is in the form of an executable code driven by an interpretive input file. Hence, the first step in the process is to convert the system noise prediction using ANOPP from the companion paper,[7] to ANOPP2 user code(s). The approach taken is depicted in Figure 9.

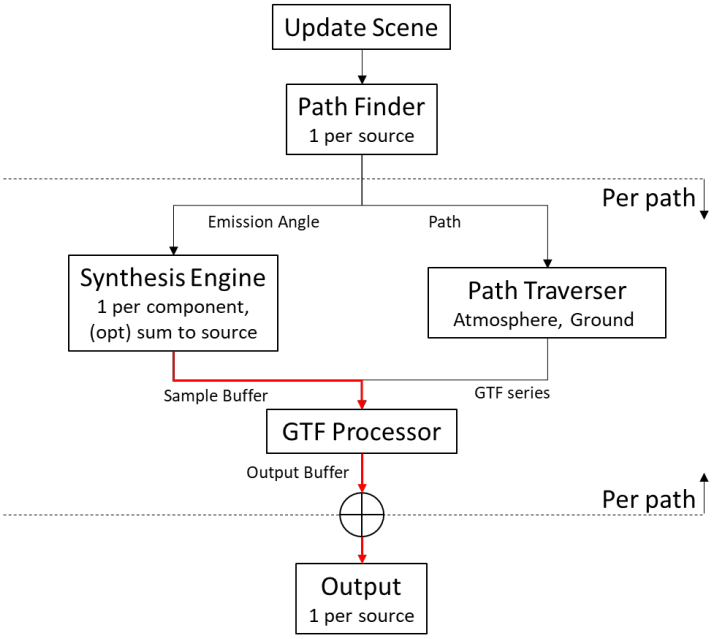

Figure 8: Flowchart depicting the typical use case of the NAF. Red lines indicate pressure time history (audio) data.

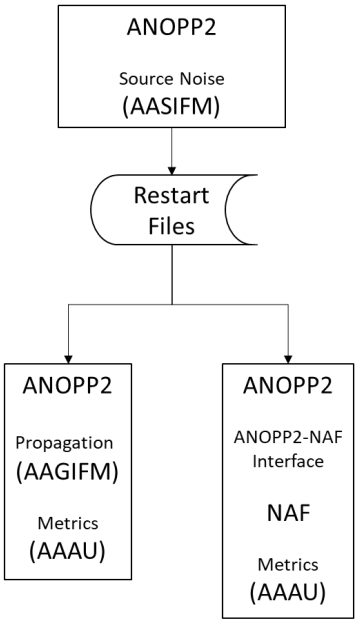

Figure 9: Flowchart depicting coupled ANOPP2-NAF simulation frameworks.

A common starting point for both the system noise prediction, shown in the left branch of Figure 9, and the auralization, shown on the right, is the generation of the source noise definition. This is accomplished with an ANOPP2 user code that calls the ANOPP2 ANOPP Source Internal Functional Module (AASIFM). Here, the AASIFM runs ANOPP to calculate the source noise at the waypoints in the prescribed flight path using the semiempirical models listed in Table 2. The noise data (inclusive of their suppressions) are in the form of one-third octave band spectra for a grid of observers at a fixed distance from the source, that is, the so-called source noise hemisphere. For auralization, tonal source data (without their suppressions) are also generated in the form of non-Doppler-shifted tonal frequencies and amplitudes at the same grid of observers. The resulting data are written to a set of restart files (one for the source noise, one for the flight path, and one for the atmosphere). In the left branch of Figure 9, a second ANOPP2 user code reads the restart files, and propagates the one-third octave band noise data to the designated ground observer using the ANOPP2 ANOPP Ground Internal Functional Module (AAGIFM). The AAGIFM runs ANOPP to propagate the noise in the frequency domain as part of a time marching simulation. In the future, this operation can be performed using the new ANOPP2 Straight Ray Propagation Internal Functional Module (ASRPIFM), which offers the capability of propagating both one-third octave band and narrowband (tonal) data. An advantage of doing so for fan rotor-stator interaction tones will be discussed in Section IV. Using AAGIFM, the results of propagation are a series of one-third octave band spectra at the ground observer at one-half second intervals.

Certification type metrics are subsequently calculated using the ANOPP2 Acoustic Analysis Utility (AAAU). Aside from differences in numerical precision, for the same input, the metrics generated by these two ANOPP2 user codes should be the same as those generated by ANOPP.

The right branch of Figure 9 shows a combined ANOPP2-NAF user code written for auralization. It first reads the restart files into ANOPP2's data structures, and transfers that information to the NAF's data structures using the ANOPP2-NAF Interface Library. From there, the NAF exercises its time marching simulation according to that depicted in Figure 8. In this work, two different NAF-APL synthesis engines are employed. The broadband synthesis engine is individually applied to each broadband component listed in Table 2. Specifically, it takes the noise hemispheres (including their suppressions), interpolates the data to the instantaneous emission angle, converts the resulting one-third octave band spectrum to a narrowband spectrum, and convolves that with random white noise in an overlap-add scheme. It should be noted here that the noise hemispheres for the engine components are reported in the ANOPP2 body reference coordinate system, and incorporate the changing angle of attack over the course of the simulation. The noise hemispheres for the airframe components, however, are reported in the ANOPP2 wind reference coordinate system, and do not incorporate the angle of attack. Therefore, an additional step is taken in the ANOPP2-NAF Interface to apply the angle of attack to the airframe components using data obtained from the Flight Path restart file. The tonal synthesis engine takes the unsuppressed tonal amplitudes for the fan rotor-stator interaction noise component, reads and applies suppression data from an external file, interpolates the resulting amplitudes to the proper emission angle, assigns a random phase to each harmonic, and synthesizes the pressure time history using an additive synthesis scheme. Referring back Figure 8, each synthesized component is propagated to the ground (i.e., no source summation for colocated components) independently for direct and ground reflected paths, then summed at the observer to obtain the pseudorecording. Certification type metrics are computed using the AAAU.

C. Differences between ANOPP/ANOPP2 and NAF

Ideally, metrics generated by ANOPP/ANOPP2 will compare well with those generated by the NAF. There are, however, differences in capabilities that may affect the level of parity achievable. These are next briefly discussed.

1. Lack of WING Analog in NAF

The WING module, used for shielding of the fan inlet noise in the ANOPP/ANOPP2 analyses, is applied as part of the propagation process. There exists no similar capability in the NAF. Previous work adopted a scheme to perform the ANOPP analyses with and without the WING module to determine a delta EPNL at the certification points. A delta gain was subsequently applied to the applicable noise hemispheres such that the EPNL computed without the WING module matched that computed with the WING module.[26] This roundabout approach was deemed unnecessary in the present work because the shielding of the broadband and tonal inlet noise was shown to be extremely effective, on the order of 50 dB in PNLT below the dominant jet noise source (see Figure 4 – Figure 7). Therefore, the broadband and tonal inlet noise were not included in the following simulations whatsoever.

2. Speed of Sound

While AAGIFM, ASRPIFM, and the NAF all perform straight line propagation, the speed of sound used by AAGIFM and ASRPIFM is determined as the average speed of sound along the path length, while that in the NAF is the average between the source and the receiver. In order to achieve parity in the following simulations, a uniform atmosphere was specified for both the ANOPP/ANOPP2 and NAF analyses, with the properties (and in particular, temperature) set to the same as those specified in the companion study (ISA+18°F) at ground level.

3. Propagation of Tonal Noise

As previously indicated, ANOPP/ANOPP2 propagate noise in the frequency domain, while the NAF does so in the time domain. In prior work,[26] the loss of phase information in the frequency domain propagation was found to affect tonal noise more than broadband noise.

4. Emission Angle Calculation

As indicated in Figure 8, the NAF Path Finder determines a separate emission angle per path per source. For straight line propagation, this results in one emission angle for direct rays and a different emission angle for ground reflected rays. The ANOPP Geometry Module (GEO) is used by AAGIFM for the computation of propagation effects. GEO determines a single emission angle for all rays. A negative consequence of that occurs when a source and observer are far above the ground, in which case the difference in emission angles between the rays is large. More relevant to this work is the case of a source and observer near the ground (during the ground roll). In the NAF, different emission angles ensure that the direct and ground reflected rays don't annihilate each other. In AAGIFM, an incoherence coefficient prevents that. Because of differences in how this condition is handled, results from

ANOPP/ANOPP2 and NAF simulations at low emission angles are expected to differ. The new ASRPIFM calculates a different emission angle for the direct and ground reflected paths.

IV. Results

A. Component Level Verification

A comparison of component level noise metrics serves as a means of verifying the implementation of the NAF in relation to the system noise prediction. Here, the focus is on the entire simulation chain, so metrics of propagated noise at a ground observer are considered, specifically at the flyover observer for the standard takeoff procedure. In the interest of isolating various propagation effects, the observer is placed flush with a hard ground and the ANSI S1.26-1995 atmospheric model[23] is used. Figure 10 – Figure 14 show comparisons of the A-weighted sound pressure level (SPL_A) and PNLT for the ANOPP/ANOPP2 system noise predictions and the NAF auralizations. In the following, broadband components were synthesized by filtering random noise and tonal components were synthesized by attributing a random phase to each component. Therefore, each realization of the simulation varies by some small amount. No effort was made to characterize the variance, but the results shown in each case were the first simulated, and not a selection of the best available. Favorable comparisons are seen for all components, that is, jet, core, combined airframe, fan exhaust broadband and tones. The fan exhaust noise is seen to be largely directed at the aft polar emission angles.

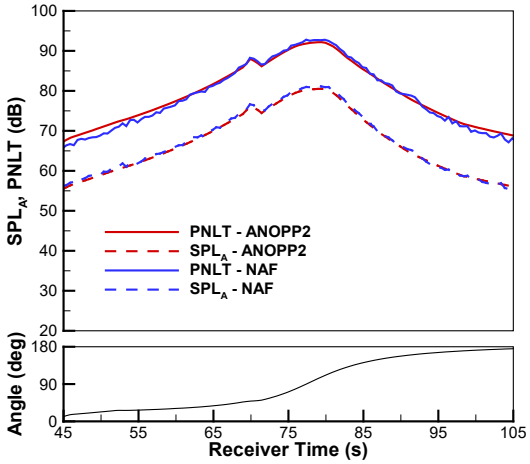

Figure 10: Jet noise metrics comparison for a standard takeoff at the flyover point.

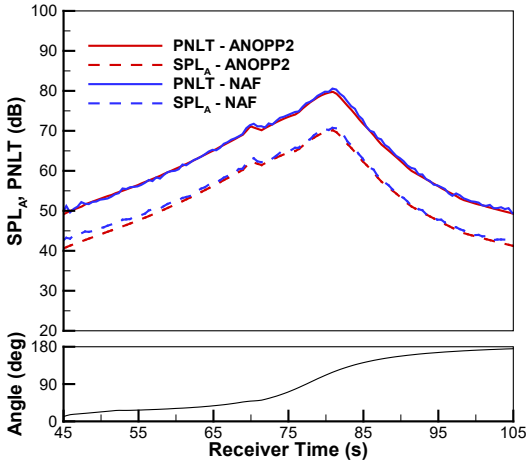

Figure 11: Core noise metrics comparison for a standard takeoff at the flyover point.

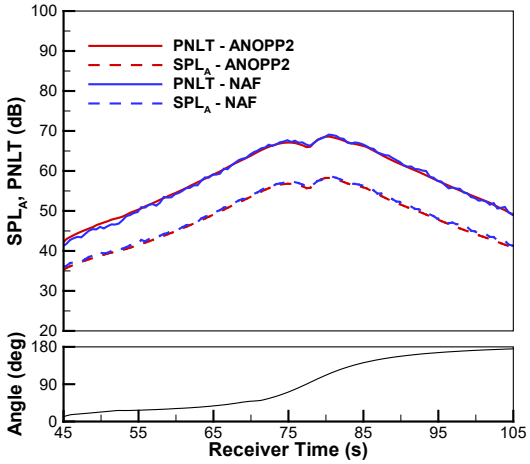

Figure 12: Combined airframe noise metrics comparison for a standard takeoff at the flyover point.

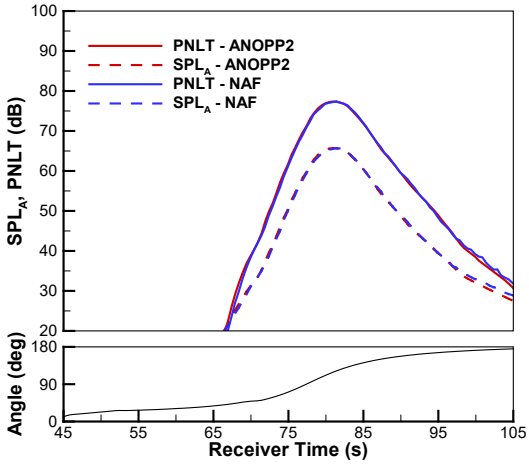

Figure 13: Fan exhaust broadband noise metrics comparison for a standard takeoff at the flyover point.

Because the aircraft noise is dominated by the jet component, and the jet noise component compares very well (Figure 10), the metrics for the total aircraft noise (all components summed) also compare very well, as seen in Figure 15. Generated pseudorecordings for each component and the total are available as sound files on the Internet.[27]

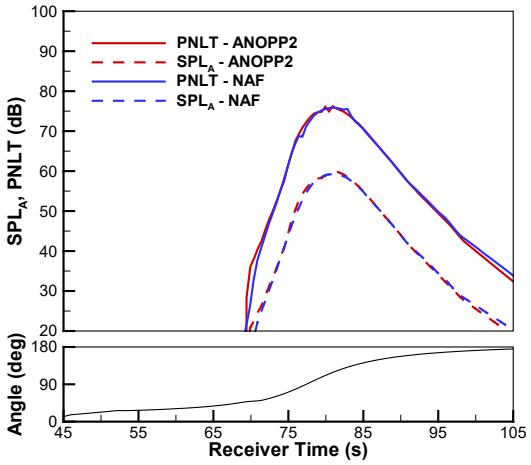

Figure 14: Fan exhaust tonal noise metrics comparison for a standard takeoff at the flyover point.

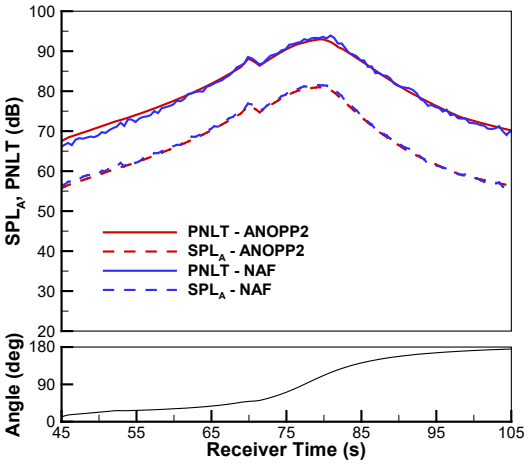

Figure 15: Total noise metrics comparison for a standard takeoff at the flyover point.

B. Propagation Effects

It is useful to consider how well the comparisons are maintained under the simulated propagation conditions of interest, namely, under the use of the SAE 866A absorption model versus the ANSI S1.26-1995 model, a finite impedance (grass) surface versus an infinite impedance (hard) surface, and a 4 ft observer height versus an observer flush with the ground. In the following, the standard takeoff procedure is considered, the observer is at the flyover point, and the propagation effects are added incrementally.

First, consider the effect of a change in the atmospheric absorption model. Figure 16 shows the comparison of PNLT of the total noise for two absorption models for an observer flush with a hard ground. The ANSI model is seen to provide slightly less absorption than the SAE model for both the system noise prediction and the auralization, resulting in EPNL differences of 0.6 and 0.5 dB, respectively.

Next, consider replacing the hard ground surface with grass (flow resistivity $\sigma = 291$ slug/s-ft^3). Here, the observer remains flush with the ground, and the SAE 866A absorption model is used. The effect is shown in Figure 17, and results in a decrease in EPNL of 1.2 dB for both the system noise prediction and the auralization, compared to the hard surface.

Finally, raising the observer to a 4 ft height above the grass covered ground has a dramatic effect, as seen in Figure 18. Not only is the EPNL significantly reduced (by about 3 dB for both the system noise prediction and auralization), but the traces become less smooth. As observed in prior works by the authors, differences in the PNLT traces (between system noise and auralization) are more pronounced for an above ground observer due to the different manners in which propagation is simulated. In the case of the system noise prediction, propagation is simulated by AAGIFM in the frequency domain, and the phase relationship between the direct and ground reflected rays is not taken into account. In contrast, the phase is retained in the auralization, so the interference between the direct and ground reflected rays is fully simulated, as shown in the spectrogram in Figure 19. The Doppler-shifted fan exhaust tones are plainly visible. Referring back to Figure 18, greater differences are noted at the low emission angles for the 4 ft observer, in part due to the different manners in which the simulations are performed, see Section III.C.4. This has little effect at higher elevation angles, and consequently, the EPNL values are unaffected. Further investigation using the ASRPIFM instead of AAGIFM is left as a future exercise.

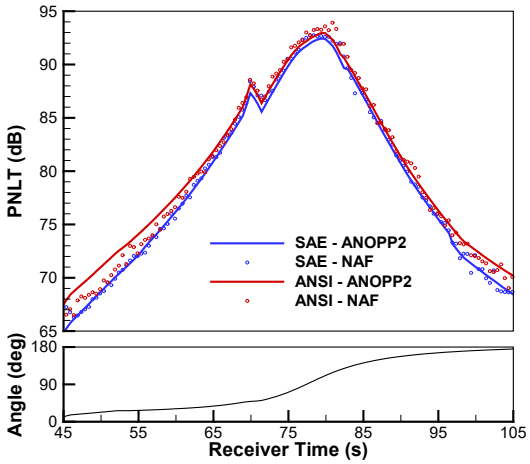

Figure 16: Comparison of total PNLT for two different atmospheric absorption models.

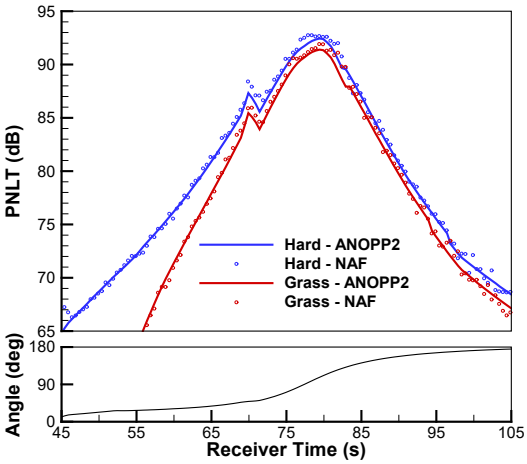

Figure 17: Comparison of total PNLT for two different ground surfaces.

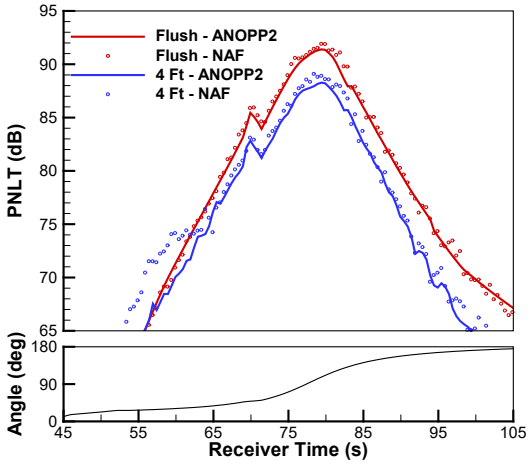

Figure 18: Comparison of total PNLT for two different observer heights.

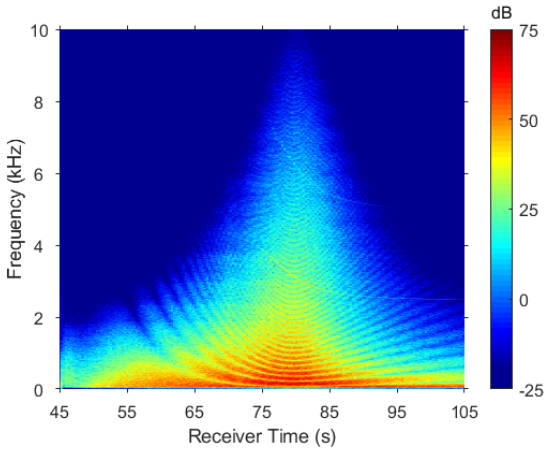

Figure 19: Spectrogram at flyover point (std. takeoff, SAE absorption, grass surface, 4 ft observer height).

C. Comparison of Standard and Advanced Takeoff Procedures

The two certification points, lateral and flyover, plus a third point located 8000 ft from brake release (shortly after rotation) and directly below the flight path are next considered. The third point was selected as a point of interest because of its potential for exhibiting significant differences between the two procedures. It is subsequently referred to as the post-rotation (PR) point and is closer to brake release than either the lateral or flyover points. In this subsection, metrics are explored in order of increasing detail, starting first with integrated metrics, and followed by metric time histories, spectrograms, and finally psychoacoustic metrics. The SAE 866A absorption model, a grass surface, and a 4 ft observer height are considered in the following simulations. Generated pseudorecordings for each procedure and location are available as sound files on the Internet.[27]

Aside from the additional measurement point, there are several differences between the system noise analyses and auralizations performed herein and the system noise analyses performed in the companion paper.[7] These include:

- The present work was performed using ANOPP2/ANOPP as described in Section III, whereas the companion work was performed exclusively using ANOPP. Small differences are expected because of loss of precision in the file input/output.
- The atmosphere is considered uniform in the present work, with conditions set to those at ground level of the lapse atmosphere (ISA+18°F) in the companion work. Differences will be greater at higher altitudes.
- A vertical offset of 13 ft (up) was applied to both the standard and advanced takeoff profiles in the present work. Without that offset, the direct and ground reflected rays in the NAF simulation effectively annihilate

each other for observers on and near the ground until the aircraft begins its climb. The companion work included no such offset. This modification makes a negligible difference in EPNL, but makes auralization of the sound from the start of the takeoff roll possible.

1. Integrated Metrics

Table 4 provides a listing of predicted EPNL values for the two takeoff procedures at the three measurement points. Very good agreement (differences no greater than ± 0.4 dB) between the system noise predictions and auralizations is seen across the range of flight conditions and measurement points. This level of agreement is typical of prior system noise analyses and auralizations conducted by the authors, and serves to verify the consistency of the two methods. Even with the analysis differences noted above, the EPNL values differ by no more than 0.4 dB between the present work and that in the companion paper, see Table 3.

Table 4: Comparison of EPNL (dB) predictions for standard and advanced takeoff procedures at three measurement points.

	Standard			Advanced			Advanced - Standard		
Method	Lateral	Flyover	PR	Lateral	Flyover	PR	Lateral	Flyover	PR
ANOPP2	94.8	88.2	111.3	92.8	86.7	113.5	-2.0	-1.5	+2.2
NAF	95.0	88.6	111.5	92.9	87.1	113.3	-2.1	-1.5	+1.8
Delta	-0.2	-0.4	-0.2	-0.1	-0.4	+0.2	+0.1	0.0	+0.4

The last three columns of Table 4 provide the differences between the advanced and standard takeoff procedures for each calculation method. While the differences are small (< ~2 dB), they are significant enough that, on a cumulative basis, the advanced procedure provides a positive noise margin and the standard procedure does not. Given that the EPNL metric takes into account both amplitude and duration, it may be difficult to discriminate the difference between takeoff procedures on the basis of EPNL alone.

2. Metric Time Histories

Metric time histories provide further insight into the differences between takeoff procedures. Figure 20 – Figure 22 provide comparisons of PNLT for both procedures. For compactness, only the auralizations are plotted; the system noise traces are comparable, except at low emission angles as previously noted. An extended timeframe is used to identify features of the takeoff procedures.

PNLT traces for the lateral measurement point are shown in Figure 20. The sudden jump in level at 10+ s is the time delay for the sound to reach the observer from the start of ground roll. Rotation occurs at about 37.5 s receiver time for the standard takeoff and at about 38.5 s for the advanced takeoff. At the 10 dB down points for the EPNL calculation, the duration of the advanced takeoff is shorter than that of the standard takeoff (due to the faster speed), and the maximum PNLT value is lower. The combined effect is a 2.1 dB reduction in EPNL. Maximum PNLT values and durations are provided in Table 5.

Figure 21 shows the PNLT traces at the flyover point. The start of the sound is further delayed as the measurement point is further downrange. Rotation occurs at about 45 s. Because the maximum PNLT values are close, most of the reduction in EPNL (1.5 dB) is due to the shorter duration of the advanced takeoff between the 10 dB down points.

At the PR point, the PNLT traces are markedly higher in amplitude and shorter in duration. The pilot-initiated cutback at around 70 s receiver time is clearly seen in Figure 22. Here, the much higher maximum PNLT of the advanced procedure outweighs the benefits of a shorter duration relative to the standard procedure, resulting in an increase in EPNL (1.8 dB) over the standard procedure.

3. Spectrograms

An additional level of detail is revealed by spectrograms of the auralizations. While a one-third octave band spectrogram may be generated from the system noise analysis results, it does not offer as fine a detail as that provided by the narrowband spectrogram generated from a pseudorecording. In addition to amplitude and duration, the spectrograms in Figure 23 provide an indication of the spectral balance and temporal character. At the lateral measurement point, the presence of the blade passage frequency (BPF) and 2BPF tones are visible. These tones are more prominent at the flyover point and not apparent at the PR point. The role of atmospheric absorption is seen by the amount of high frequency attenuation. There is very little atmospheric absorption at the closest point (PR), more at the lateral point, and still more at the flyover point. Interference patterns caused by the superposition of direct and ground reflected waves are prominent.

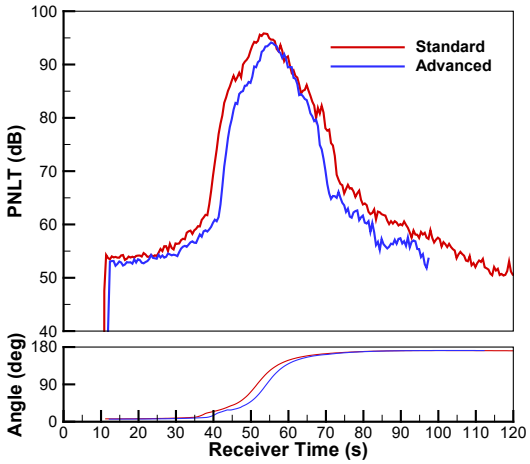

Figure 20: Comparison of total PNLT at the lateral measurement point.

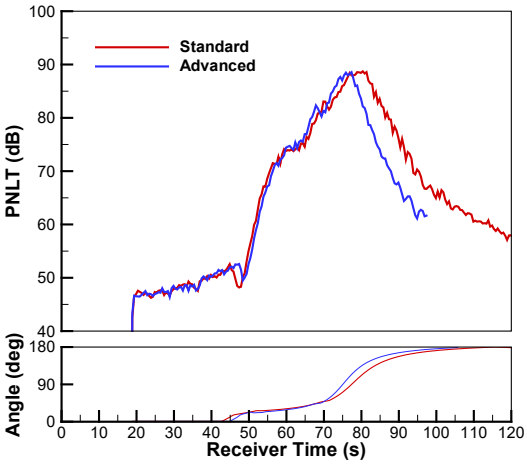

Figure 21: Comparison of total PNLT at the flyover measurement point.

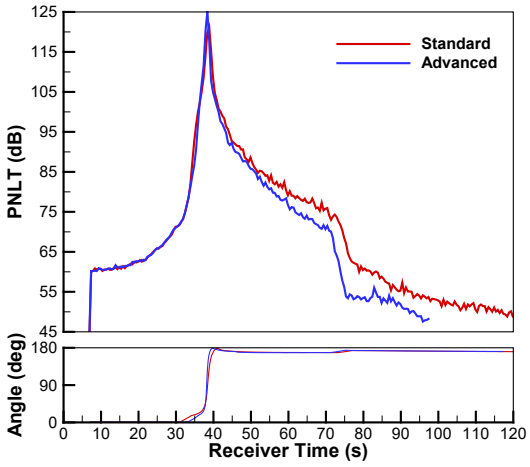

Figure 22: Comparison of total PNLT at the PR measurement point.

Table 5: Comparison of $PNLT_{max}$ and duration for standard and advanced takeoff procedures.

Measurement Point	Standard / Advanced	
	$PNLT_{max}$ (dB)	Duration (s)
Lateral	95.7 / 94.1	17.0 / 15.5
Flyover	88.2 / 87.6	21.5 / 17.5
PR	122.4 / 127.1	1.8 / 0.9

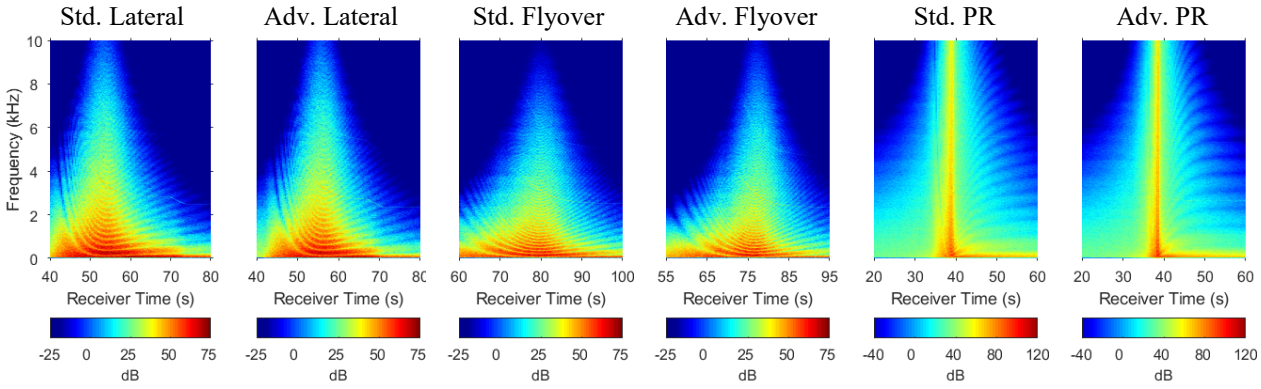

Figure 23: Spectrograms for standard and advanced takeoff procedures at three measurement points.

4. Psychoacoustic Metrics

Psychoacoustic, or sound quality, metrics offer an additional means of describing level, spectral and temporal content. Four metrics are considered: the time-varying loudness *N(t)* in sone, the time-varying sharpness *S(t)* in acum, the time-varying roughness *R(t)* in asper, and time-varying fluctuation strength *F(t)* in vacil. Time-varying loudness

reflects the human perception of the magnitude of the sound over time and is a function of the amplitude and frequency. Sharpness is an indicator of the spectral balance of a signal; the greater the amount of high frequency content, the greater the sharpness value. Roughness reflects the perception of rapid (15-300 Hz) amplitude modulation, with a maximum impression reached when loudness fluctuations are about 70 Hz. Finally, fluctuation strength is similar to roughness, but reflects perception of slow fluctuations (1-16 Hz), with a maximum effect at about 4 Hz. The metrics were computed as described in prior work by the first author.[28]

One means of relating the sound quality metrics to the EPNL certification metric is through the Psychoacoustic Annoyance (PA) model, described by Zwicker and Fastl.[29] The PA model offers a quantitative value of annoyance and is based on psychoacoustic tests using narrowband and broadband sounds having different spectral and temporal characteristics. A time-varying form is given by

$$PA(t) = N(t)\left[1 + \sqrt{w_s^2(t) + w_{FR}^2(t)}\right] \tag{1}$$

in which

$$w_s(t) = \begin{cases} 0.25\,(S(t) - 1.75)\log_{10}(N(t) + 10) & \text{for} \quad S > 1.75 \\ 0 & \text{for} \quad S \le 1.75 \end{cases} \tag{2}$$

$$w_{FR}(t) = \frac{2.18}{N(t)^{0.4}}\left[0.4F(t) + 0.6R(t)\right] \tag{3}$$

For the auralization of standard and advanced takeoff procedures at the three measurement points, the values of roughness, sharpness, and fluctuation strength were low. Hence, for the cases considered herein, the psychoacoustic annoyance, as expressed by Eq. (1), is loudness dominated.

Calculation of psychoacoustic annoyance can be performed in one of two ways: on a time-varying basis or on an integrated basis. In the former, direct application of Eq. (1) results in a *PA* time history. In the latter, metric percentiles may be used to provide a single *PA* value. Zwicker and Fastl's original form of Eq. (1) used the 5th percentile of loudness (N_5), that is, the value of loudness that is exceeded 5% of the measurement time. However, the authors were not specific with respect to the percentiles for sharpness, roughness, and fluctuation strength. Consequently, two alternative methods for calculating PA_5 were exercised. In the first, PA_5 was computed directly from the *PA* time history. In the second, PA_5 was computed using the 5th percentiles of the individual metrics, that is, N_5, R_5 and F_5, in lieu of *N(t)*, *R(t)* and *F(t)*. For all six auralizations, the two methods yielded nearly the same values. Those obtained from the second method were used in the following.

A benefit of using percentiles is that the event duration is implicitly taken into account. However, unlike the standardized EPNL calculation, which integrates PNLT between the 10 dB down points on either side of the peak value, there is no standard for choosing the event duration for calculation of the 5th percentiles. As the current use of the Psychoacoustic Annoyance model is intended to evaluate relative annoyance, the duration is somewhat arbitrary as long as it is consistent between sounds. In this work, a duration ranging from 20 s on either side of peak *PA(t)* was chosen, for a total record length of 40 s. Figure 24 provides comparisons of *PA(t)* for the standard and advanced takeoff procedures at the three measurement points. These are used in the first method of computing PA_5. It is seen that *PA(t)* data are comparable in character but differ at each measurement point, and vary significantly between measurement points. Plots of *N(t)*, *R(t)* and *F(t)* are omitted for brevity.

The percentile representation of *PA*, like EPNL, incorporates duration, level, and spectral content. Therefore, it is of interest to determine if a relationship exists between EPNL and PA_5. Since EPNL is on a logarithmic scale and *PA* is essentially linear in sone, a linear regression was performed between EPNL and $\log_{10}(PA_5)$. Figure 25 shows the least squares regression line when all six auralizations are included in the regression. Here, each plot symbol refers to a particular auralization; symbols 1, 2, and 3 refer to the lateral, flyover, and PR measurement points for the standard procedure, respectively, and symbols 4, 5, and 6, refer to the same three measurement points for the advanced procedure. According to the psychoacoustic annoyance model, the advanced procedure is less annoying than the standard procedure at the lateral and flyover points, and more annoying at the PR point. The fact that PA_5 accounts for 99% of the variance seen in EPNL is remarkable. If the psychoacoustic annoyance model is a good predictor of annoyance for this set of sounds, then EPNL would be as well.

V. Concluding Remarks

Auralizations of a supersonic technology concept airplane were performed using source noise definitions from system noise analyses for standard and advanced takeoff procedures. The system noise predictions were regenerated using NASA's second generation Aircraft Noise Prediction Program (ANOPP2) in a manner that was consistent with

predictions made in a companion paper[7] using ANOPP. These analyses demonstrated that the advanced procedure, employing a high-speed climbout and a programmed thrust lapse rate of 10%, could reduce the noise at the lateral and flyover measurement points. Auralizations were made possible by coupling ANOPP2 with the NASA Auralization Framework (NAF).

The auralizations were made consistent with the system noise predictions through the use of the same or similar propagation capabilities. Some variances, particularly at low emission angles, were observed, but did not impact the integrated metric EPNL. Additional measures of the resulting pseudorecordings were made to highlight differences in amplitude, duration, and spectra. A psychoacoustics model based on sound quality metrics was used to predict possible human annoyance, and was found to explain nearly all of the variance seen in EPNL. This suggests that EPNL would be a good indicator of annoyance if the annoyance model is accurate. For now, that remains an open question.

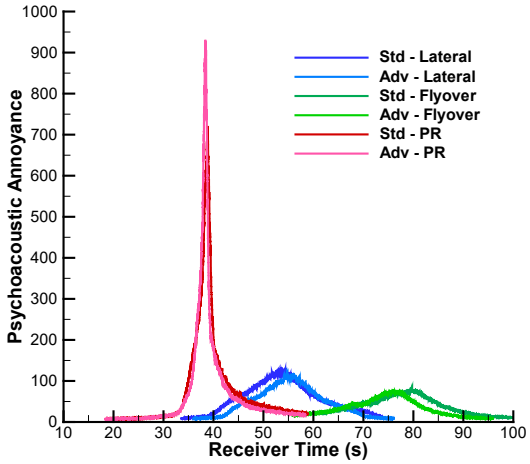

Figure 24: Comparison of psychoacoustic annoyance.

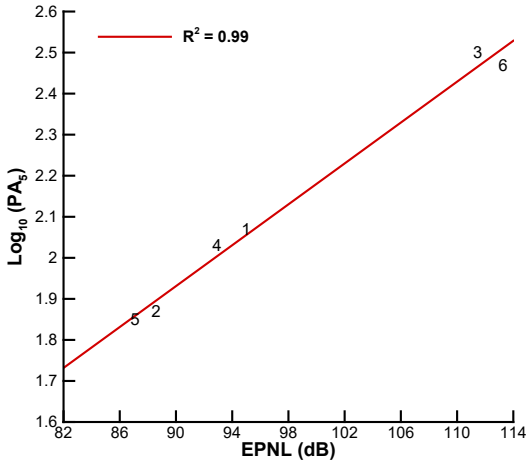

Figure 25: Linear regression between EPNL and PA_5.

Acknowledgments

This work was funded by the NASA Commercial Supersonic Technology Project and the NASA Transformational Tools and Technologies Project. Special thanks are given to the NASA Langley ANOPP2 team (Venkat Iyer, Jeremy Jones, and Leonard Lopes) for translating the original ANOPP input decks into an ANOPP2 user code in C++ and for providing ANOPP2 technical support, and to Aric Aumann for assisting with new NAF developments and for providing NAF technical support.

References

[1]Maglieri, D.J., Bobbitt, P.J., Plotkin, K.J., Shepherd, K.P., Coen, P.G., and Richwine, D.M., "Sonic boom, Six decades of research," NASA SP-2014-622, 2014.

[2]Berton, J.J., Jones, S.M., Seidel, J.A., and Huff, D.L., "Noise predictions for a supersonic business jet using advanced take-off procedures," *The Aeronautical Journal*, Vol. 122, No. 1250, 2018, pp. 556-571.

[3]Grantham, W.D. and Smith, P.M., "Development of SCR aircraft takeoff and landing procedures for community noise abatement and their impact on flight safety," *Supersonic cruise research*, NASA CP 2108, 1979, pp. 299-333.

[4]Zorumski, W.E., "Aircraft noise prediction program theoretical manual," NASA TM-83199, 1982.

[5]Rizzi, S.A. and Sahai, A.K., "Auralization of air vehicle noise for community noise assessment," *CEAS Aeronautical Journal*, Vol. 10, No. 1, 2019, pp. 313-334.

[6]Aumann, A.R., Tuttle, B.C., Chapin, W.L., and Rizzi, S.A., "The NASA Auralization Framework and plugin architecture," *InterNoise 2015*, San Francisco, CA, 2015.

[7]Berton, J.J., Huff, D.L., Seidel, J.A., and Geiselhart, K.A., "Supersonic technology concept aeroplanes for environmental studies," *AIAA SciTech Forum*, Orlando, FL, 2020.

[8]"ARP 866 Rev. A, Standard values of atmospheric absorption as a function of temperature and humidity," SAE International, Warrendale, PA, 1975.

[9]Lopes, L.V. and Burley, C.L., "ANOPP2 User's Manual: Version 1.2," NASA TM-2016-219342, 2016.
[10]Claus, R.W., Evans, A.L., Lylte, J.K., and Nichols, L.D., "Numerical Propulsion System Simulation," *Computing Systems in Engineering*, Vol. 2, No. 4, 1991, pp. 357-364.
[11]"Annex 16 to the Convention on International Civil Aviation, Environmental Protection, Volume I, Aircraft Noise (7th Edition)," International Civil Aviation Organization, Montreal, Canada, July 2014.
[12]"ARP 876, Gas turbine jet exhaust noise prediction," SAE International, Warrendale, PA, 1978.
[13]Kontos, K.B., Janardan, N., and Gliebe, P.R., "Improved NASA-ANOPP noise prediction computer code for advanced subsonic propulsion systems. Volume 1: ANOPP evaluation and fan noise model improvement," NASA CR-195480, October 1996.
[14]Kontos, K.B., Kraft, R.E., and Gliebe, P.R., "Improved NASA-ANOPP noise prediction computer code for advanced subsonic propulsion systems. Volume 2: Fan suppression model development," NASA CR-202309, December 1996.
[15]Maekawa, Z., *Memoirs of the Faculty of Engineering*, Noise reduction by screens. 1966, Kobe University, Kobe, Japan. p. 472-479.
[16]Hough, J.W. and Weir, D.S., "Aircraft noise prediction program (ANOPP) fan noise prediction for small engines," NASA CR-198300, October 1996.
[17]Emmerling, J.J., Kazin, S.B., and Matta, R.K., "Core engine noise control program. Volume III, Supplement 1 - Prediction methods," FAA-RD-74-125, III-I (Available from DTIC as AD A030 376), March 1976.
[18]Fink, M., "Airframe noise prediction method " U.S. Department of Transportation, Federal Aviation Administration, FAA-RD 77-29, 1977.
[19]Herkes, W. and Stoker, R., "Wind tunnel measurements of the airframe noise of a high-speed civil transport," *36th AIAA Aerospace Sciences Meeting and Exhibit*, AIAA-98-0472, Reno, NV, 1998.
[20]Rawls Jr., J.W. and Yeager, J.C., "High speed research noise prediction code (HSRNOISE) user's and theoretical manual," NASA CR-2004-213014, December 2004.
[21]Chien, C.F. and Soroka, W.W., "Sound propagation along an impedance plane," *Journal of Sound and Vibration*, Vol. 43, No. 1, 1975, pp. 9-20.
[22]Embleton, T.F.W., Piercy, J.E., and Daigle, G.A., "Effective flow resistivity of ground surfaces determined by acoustical measurements," *The Journal of the Acoustical Society of America*, Vol. 74, No. 4, 1983, pp. 1239-1244.
[23]"American National Standard, Method for the calculation of the absorption of sound by the atmosphere," Acoustical Society of America, ANSI S1.26-1995 (ASA 113-1995), 1995.
[24]Rizzi, S.A. and Sullivan, B.M., "Synthesis of virtual environments for aircraft community noise impact studies," *11th AIAA/CEAS Aeroacoustics Conference*, AIAA-2005-2983, Monterey, CA, 2005.
[25]Tuttle, B.C., Aumann, A.R., Rizzi, S.A., Jones, J., and Lopes, L.V., "Flyover noise simulation using NASA's coupled aircraft system noise prediction and auralization frameworks," *Noise-Con 2017*, Paper 347, Grand Rapids, 2017.
[26]Rizzi, S.A., Aumann, A.R., Lopes, L.V., and Burley, C.L., "Auralization of hybrid wing-body aircraft flyover noise from system noise predictions," *AIAA Journal of Aircraft*, Vol. 51, No. 6, 2014, pp. 1914-1926.
[27]http://stabserv.larc.nasa.gov/flyover/, NASA, 2019.
[28]Rizzi, S.A., Burley, C.L., and Thomas, R.H., "Auralization of NASA N+2 aircraft concepts from system noise predictions," *22nd AIAA/CEAS Aeroacoustics Conference*, AIAA 2016-2906, Lyon, France, 2016.
[29]Zwicker, E. and Fastl, H. Second ed, Psychoacoustics, Facts and Models, ed. M.R. Schroeder. Springer-Verlag, Berlin, 1999.